Existence of two twinning-mediated plastic deformation modes in Au nanowhiskers

Andreas Sedlmayr [a], Erik Bitzek [b], Daniel S. Gianola [c], Gunther Richter [d], Reiner Mönig [a,*], Oliver Kraft [a]

[a] *Institute for Applied Materials, Karlsruhe Institute of Technology, Hermann-von-Helmhotz-Platz 1, 76344 Eggenstein-Leopoldshafen, Germany*
[b] *Institute I: General Materials Properties, Department of Materials Science and Engineering, Friedrich-Alexander-Universität Erlangen-Nürnberg, Martensstr. 5, 91058 Erlangen, Germany*
[c] *Department of Materials Science and Engineering, University of Pennsylvania, 3231 Walnut Street, Philadelphia, PA, USA*
[d] *Max-Planck-Institute for Intelligent Systems, Heisenbergstr. 3, 70569 Stuttgart, Germany*

Abstract

We have performed in situ scanning electron microscopy tensile experiments and molecular dynamics (MD) simulations on nominally defect-free single-crystalline Au nanowhiskers. The room temperature experiments reveal strengths on the order of the ideal strength and plastic strains of up to 12%, a direct result of deformation twinning that governs plastic flow. The in situ and post mortem electron microscopy observations can be divided into two broad classes of deformation morphologies that correlate with distinct stress–strain responses. MD simulations show that the mechanism of twin growth can change from layer-by-layer propagation to parallel and accelerated formation of coalescing nanotwins. The transition between mechanisms is caused by the bending moment resulting from the augmented stress state due to the initial twin and the boundary conditions when a twin grows beyond an embryonic state. These distinct manifestations of deformation twinning suggest that nanoscale material behavior can be tailored for high tensile ductility in addition to ultra-high strength.
© 2012 Acta Materialia Inc. Published by Elsevier Ltd. All rights reserved.

Keywords: Nanowire; Deformation twinning; In situ tension test; Scanning electron microscopy (SEM); Atomistic simulation

1. Introduction

In face-centered cubic (fcc) metals, ordinary dislocation plasticity (ODP) occurs by successive propagation of two partial dislocations with different Burgers vectors (b_p) on the same slip plane, which produce slip with Burgers vector of a full dislocation b at stresses that are a small fraction of the theoretical shear strength of the crystal [1]. An alternative deformation mechanism to ODP is deformation twinning (DT), in which the crystal is sheared by a fixed amount ($\gamma = 0.707$ for cubic crystals) by the cooperative motion of twinning partial dislocations with the same Burgers vector on adjacent crystallographic planes. In fcc metals, DT and ODP are usually seen as competing processes, with DT only being favorable for deformation at high strain rates and/or low temperatures [2]. However, plastic deformation in nanoscale volumes is markedly different than in its macroscopic counterparts, and recent experiments on nanocrystalline (nc) as well as single crystalline nanoscale fcc metals have shown DT operating at room temperature and typical experimental strain rates [3–8]. The crossover from ODP to DT has been attributed to the competition between the high stresses required to bow a full dislocation across a nanoscale grain or volume and the energy penalty of forming planar stacking faults required for the commencement of twinning [3]; thus

* Corresponding author. Tel.: +49 721 608 22487; fax: +49 721 608 22347.
E-mail address: reiner.moenig@kit.edu (R. Mönig).

leading to a size dependence of the operative deformation mechanism. In addition to the creation of an initial stacking fault, on which a two-layer thick twin embryo can form [9], twinning dislocations must be stimulated on adjacent glide planes to propagate the twin boundary and increase the size of the twin [8]. The probability for this "stimulated slip" depends on the mechanism of twin propagation; examples include a pole mechanism [8] or grain boundary processes [10,11]. In contrast to nc polycrystals, investigations of twinning in single crystalline fcc metals have been mostly [5–7] limited to atomistic simulations [12–18], which are confined to small crystal sizes and high strain rates. Here, we report quantitative in situ tensile experiments in the scanning electron microscope (SEM) on individual gold nanowhiskers and use molecular dynamics (MD) simulations to rationalize the observed DT-mediated deformation modes.

2. Methods

2.1. Experimental procedure

Individual Au nanowhiskers with diameters between 40 and 200 nm were tested in tension. The nanowhiskers are single-crystalline, high-aspect-ratio structures with a $\langle 110 \rangle$ axial orientation, which are synthesized via physical vapor deposition under molecular beam epitaxy conditions. This process leads to high crystalline quality and faceted morphology. Details on the synthesis and characterization of these nanowhiskers can be found in Ref. [19]. Quantitative tensile testing was performed in an SEM to provide real-time information about deformation morphology, but also to aid with precise alignment and local strain measurement of testing specimens. All experiments were conducted in vacuum ($\sim 10^{-6}$ mbar), at room temperature, and at quasi-static strain rates ($\sim 10^{-4}$ s^{-1}). Details of the test setup can be found in Refs. [20,21]. Proper alignment of a nanowire specimen with respect to both the force measurement and actuation axis is critical for precise mechanical characterization and understanding of the underlying deformation mechanisms. Such alignment must be verified using the limited visual feedback available in the SEM. There are two distinct routes to elucidate the alignment before harvesting: (i) tilting the microscope stage with the specimen at the eucentric height and its axis perpendicular to the tilting axis, and (ii) acquiring a single frame of the ion beam which is at an inclined angle. When tilting in both directions the projection of a properly aligned wire in the focal plane should be longest at 0° and subsequently shorten upon tilting in either direction. While tilting before harvesting was frequently used, utilization of the ion beam was avoided to not damage the specimens.

2.2. Simulation set-up

The MD simulations were performed using [1 0 1] oriented nanowhiskers with hexagonal cross-sections, as shown in Fig. 1a, which were modeled after experimentally determined nanowhisker shapes [19]. Periodic boundary conditions were used in the direction of the tensile (x) axis with a box length of $L = 288$ nm. The diameter of the whiskers was $d = 13$ nm. The perfect whisker shown in Fig. 1b was equilibrated after structural optimization using FIRE [22] for 80 ps at 300 K using standard MD, followed by 120 ps using the Nosé–Hoover [23] thermostat and barostat along the periodic axis to relax possible stresses along the tensile axis. In addition to the perfect whisker in Fig. 1a and b, two other whiskers of identical geometry and size were studied: a whisker containing two stacking faults introduced by pre-deformation (Fig. 1c) and a whisker with rough surfaces (Fig. 1d). The pre-deformed whisker was obtained from the perfect whisker by taking a configuration after 4.5% tensile straining at 300 K and 10^8 s^{-1}. This configuration shortly after the onset of plastic deformation contains two stacking faults. It is subsequently scaled back to a configuration of zero stress and equilibrated for 200 ps at 300 K. The whisker with rough surfaces was produced by randomly removing two-thirds of the atoms in the two outermost surface layers of the perfect whisker, followed by an equilibration at 600 K for 10 ps and a quenching by FIRE to an equilibrium configuration. This was subsequently also equilibrated at 300 K and zero stress for 200 ps. Tensile deformation was applied by homogeneously straining the whiskers and the simulation box in the x-direction at a rate of 10^8 s^{-1}, while controlling the temperature with the Nosé–Hoover thermostat [23]. The atomic interaction is modeled by the EAM potential for Au described in Park et al. [24]. The simulation results were analyzed using the dislocation extraction algorithm DXA
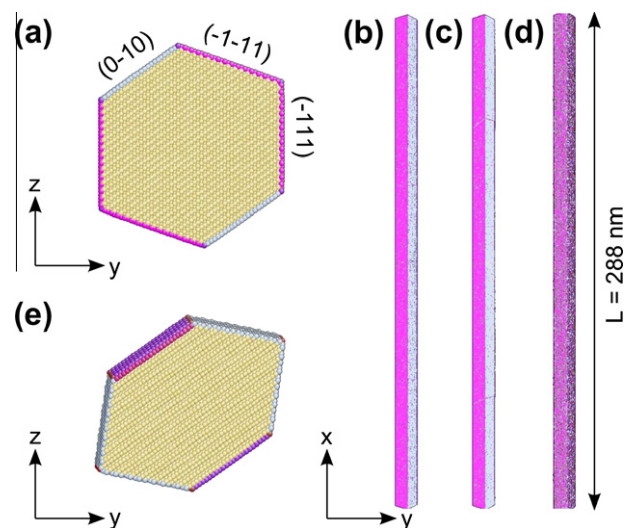

Fig. 1. (a) Cross-section of the simulated whiskers; (b) pristine whisker; (c) pre-deformed whisker containing two stacking faults; (d) whisker with rough surface; (e) cross-section of the whisker after deformation twinning on the $(-1\,1\,-1)$ plane in $[1\,2\,1]$ direction. The color denotes the coordination number: yellow: 12; magenta: 9; grey: 8. (For interpretation of the references to colour in this figure legend, the reader is referred to the web version of this article.)

by Stukowski [25] and according to the coordination number and the centrosymmetry parameter [26].

3. Results

3.1. Experimental results

In the experiments, the nanowhiskers showed elastic–plastic transitions at high stresses (ranging from 0.6 to 1.6 GPa) with significant variations in their detailed mechanical response and plastic morphology, as shown in Fig. 2. Following a period of elastic loading, the onset of plasticity is correlated with the formation of discrete slip steps that provide surface offsets that can be observed in SEM images (Fig. 2c and d). Subsequent testing exhibited significant variation in deformation behavior. Stress–strain data and corresponding morphology obtained from 28 whiskers delineate two distinct classes of behavior. In class I, plasticity occurred in a continuous fashion as demonstrated by smooth transitions to flow and the absence of large intermittent load drops (Fig. 2a). SEM images corroborate the suppression of strong plastic localization during this flow regime. In these whiskers, the slip steps appeared at various locations along the whisker on multiple slip systems. During the course of plastic flow, which maintained high stresses (Fig. 2a), additional steps formed at new sites along the whisker. Failure often occurred abruptly and the regions near the fracture sites showed various amounts of necking.

In class II, deformation was localized, which was characterized by extended thinned regions that formed before final failure. Here, no or only limited yielding occurred at stresses comparable to the yield stresses of class I. Instead, stress drops occurred and subsequent flow at significantly reduced stresses (between about 0.4 and 0.7 GPa) took place, see Fig. 2b. These stress drops were correlated with the formation of thinned regions. After rupture, which occurred at the interface separating the thinned region from the parent whisker, this region tilted to the side, forming a characteristic angle relative to the initial whisker axis (Fig. 2d). The lengths of the thinned regions exhibited a broad distribution, but were typically several times larger than the width of the whisker. A movie highlighting this class of deformation is shown in the Supporting information (Movie M1).

Electron backscattered diffraction (EBSD) analysis was performed at the fracture sites of eight whiskers belonging to both classes to determine the site-specific crystal orientation. In all cases except for one, the regions near fracture sites showed a twin orientation relationship relative to the parent crystal (corresponding to a change in the tensile orientation from [101] to [−1−14]). Figs. 3b and c show detailed EBSD data from a tested whisker belonging to class II. The parent whisker had a [101] orientation along the tensile (x) axis (Fig. 3a) with a narrow distribution of orientation. The deformed regions appeared as twins in the EBSD data and had a spread in crystal orientation of ∼10° between regions labeled "2" and "4". Within these regions, the orientation of the whisker showed a gradual change. As shown in Fig. 3c, this orientation spread only manifested about the tensile axis, with little detectable spread in the orthogonal direction. Region "3" denotes a
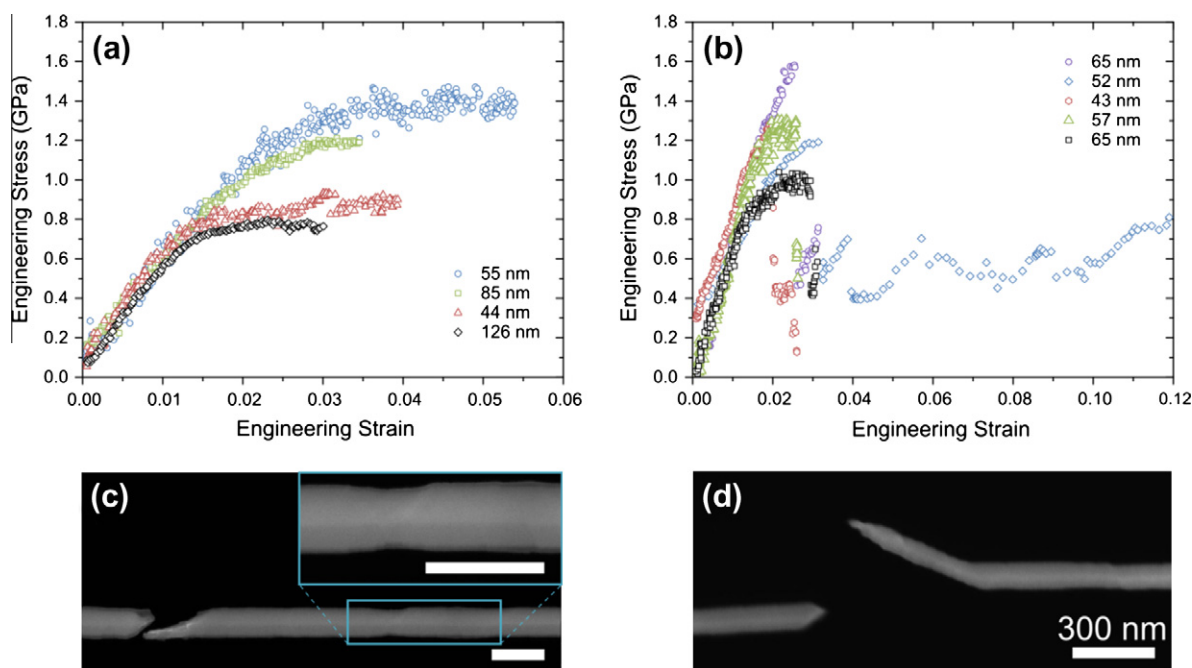

Fig. 2. The two classes of deformation behavior, each with stress–strain curves and SEM micrograph after failure (the stress–strain curves corresponding to the images are black). Characteristic stress–strain curves of class I (a) show significant plasticity at the level of yield. Deformation is accompanied by the formation of many small slip steps on multiple slip systems (c). For class II (b) the stress drops after yield and varying amounts of plastic flow are observed. Stress drops can be correlated with extended thinned regions, which tilt away from the tensile direction after fracture (d).
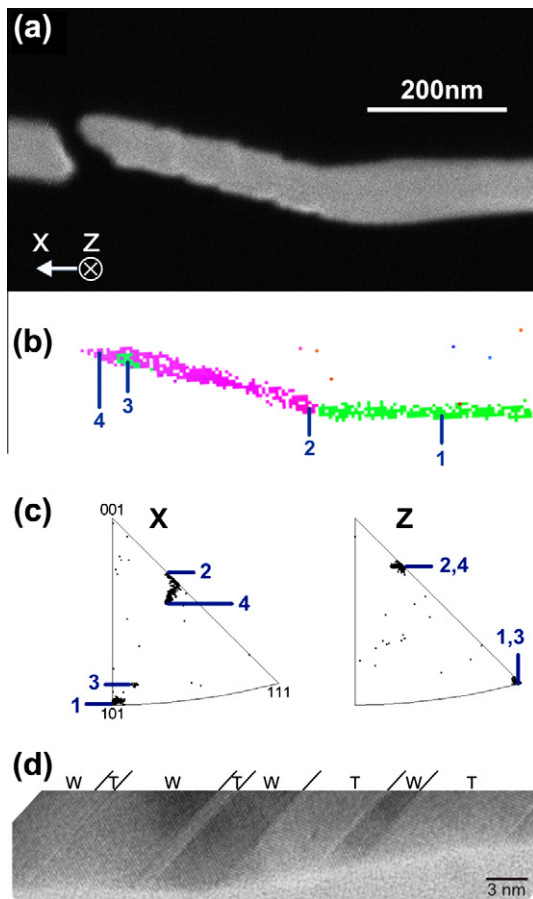
Fig. 3. EBSD and TEM observations of twinning according to class II. The mechanical response of the illustrated specimen corresponds to the green stress–strain curve in Fig. 2b. SEM micrograph shows the tilted region at the fracture site of the specimen (a). The inverse pole figure map (b) clearly illustrates the twin relationship between the undeformed (green) and deformed (pink) region. Numbered spots belong to distinct positions in the inverse pole figure (c). It can be seen that the parent whisker had a [1 0 1] orientation along the tensile axis (x). The deformed region exhibits a gradual change of ~10° in crystal orientation between "2" and "4". In (d) a high resolution TEM image shows several twinned regions (T) in the matrix of the whisker (W), formed during the deformation process. The stress–strain curve and an SEM image of this particular whisker are shown in Fig. 2b (black curve) and Fig. 2d respectively. (For interpretation of the references to colour in this figure legend, the reader is referred to the web version of this article.)

volume that has an orientation close to that of the undeformed region. Fig. 3d shows a high resolution transmission electron microscopy (TEM) image, corresponding to the black stress–strain curve in Fig. 2b and the SEM image in Fig. 2d, showing twin lamellae that formed during the deformation process where several twinned regions are clearly visible. All twin boundaries were identified as Σ3 (1 1 1)[1 0 −1] type symmetric tilt grain boundaries.

After tensile testing, the alignment of the nanowhiskers in the focal plane was verified. This was accomplished during the EBSD measurements, in which the sample is tilted to 70° with respect to the e-beam axis. The substrate on which the fractured specimens were mounted was rotated so that its axis was coaxial with the tilt axis of the

microscope stage and deviations from uniaxial alignment could be readily observed by incrementally tilting. Fig. 4 shows two SEM micrographs, which were recorded at a tilt of 70°. Proper alignment can be observed for three wires in Fig. 4a, whereas two wires show strong misalignment and therefore their data were not used. Fig. 4b shows the alignment of a wire at 0° (see inset) and 70° with no change in the focal plane. Both classes of deformation morphology, as described in the main text, are observed for proper alignment, showing that the existence of the two distinct classes of mechanical behavior is not caused by misalignment.

3.2. Simulation results

MD simulations confirmed that Au whiskers of similar shape and identical orientation as in the experiments deformed predominantly by twinning. This behavior was also found when other EAM potentials for gold or different strain rates or whisker sizes were used [27]. Snapshots of the different whiskers are shown in Fig. 5, and movies of the deforming nanowhiskers are provided in the Supporting information (Movies M2–M4). In these snapshots and movies, the twinned regions are clearly identified by the color of the atoms (indicating the coordination number of the surface atoms) which changes from magenta to grey, showing surface reorientation by twinning from {1 1 1} to {1 0 0} surfaces. Similarly, the {1 0 0} surfaces transformed to {1 1 0} surfaces as a result of twinning. In the twinned regions, the wire axis direction changed from [1 0 1] to [−1 −1 4]. It is important to note that the periodic boundary conditions accommodated the reorientation of the twinned regions by rotation, such that the tensile axis became a ⟨0 0 1⟩-direction in the twinned parts. As a result of the twinning, the whisker cross-section changed from a truncated rhombic to a truncated square cross-section, see Fig. 1e. The stress–strain curves are shown in Fig. 6. The initially defect-free whisker failed at 16% strain at the intersection of two oppositely oriented twins. The pre-deformed whisker also failed at the intersection of two opposite twins; however, the twins were longer and the whisker accommodated more strain (32%). Similar to the experiments, the twinned region tilted away from the whisker axis following rupture, as shown in Fig. 5. In the whisker with rough surfaces, only two large twins formed which spread nearly completely through the entire whisker. This sample failed at 59% strain.

A more detailed analysis of the initial stages of plastic deformation shows that the first leading partial dislocations nucleated at a corner between a {1 1 1} and a {1 0 0} surface, see Fig. 7a. Other leading partial dislocations were nucleated where a dislocation cut the surface to create a step (Fig. 7b). In particular, leading dislocations of the same Burgers vector were often generated on atomically adjacent parallel planes where the dislocation intersected the corners between surfaces (see Fig. 7a–d and Movie M5). These twinning dislocations glided on the original stacking fault and thus formed a two-layer embryonic twin.
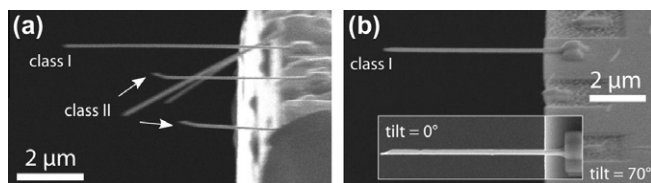
Fig. 4. SEM micrographs of fractured nanowhiskers. For the EBSD measurements the substrate is aligned coaxial to the tilt axis of the microscope stage. By subsequent tilting the specimens are checked for misalignment. (a and b) Show both classes of deformation behavior for properly aligned wires, which confirms that the existence of the two distinct classes is not caused by misalignment.

Fig. 6. Engineering stress–engineering strain response for the three different whiskers simulated at 300 K with a strain rate of $10^8 \, s^{-1}$.

While doing so, they cut the surface edges and thus led to the generation of more twinning dislocations on the adjacent plane, further propagating the twin boundary in a self-stimulating fashion. The entire process took place simultaneously on both sides of the initial stacking fault. Also, one leading partial dislocation generated twinning dislocations at multiple corners on the same parallel glide plane. These then combined on top of the fault left by the generating dislocation. One key feature is that the stimulated nucleation of twinning dislocations can take place at several corners, making the propagation mechanism of the twin boundary highly redundant.

When the twins got longer, a second propagation mechanism was observed: the emission of multiple partial dislocations ahead of the twin boundary which have Burgers vectors and glide planes identical to the twinning dislocations of the twin (see Fig. 7e–h and Movie M6). The nucleation of these dislocations was most likely caused by the bending moment induced by the twin in combination with the boundary conditions. On each of these partial dislocations embryonic twins formed and grew, eventually leading to the coalescence of these twins with each other and the main twin. Fig. 7e–h shows such concentrated zones of dislocation nucleation and the formation of twin embryos that led the propagating twin front, which we call leapfrogging events. The parallel development of many twins thereby
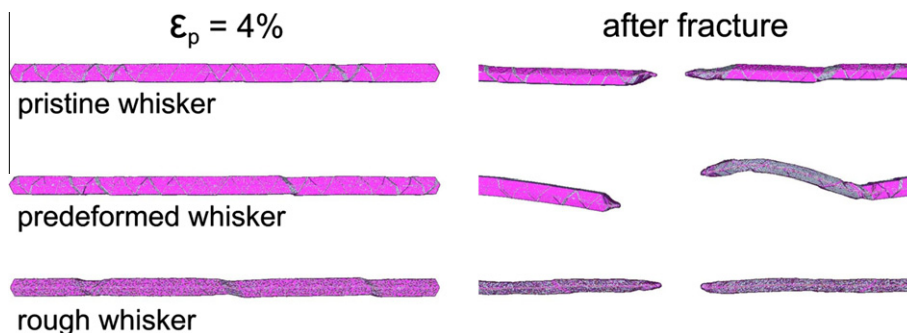
leads to faster propagation of the twinned region compared to the layer-by-layer propagation of one twin boundary.

4. Discussion

Experimental observations of deformation twinning in similar Au whiskers have also recently been reported [5–7]. MD simulations of smaller, $\langle 1\,1\,0 \rangle$ oriented fcc nanowhiskers also show deformation twinning, where this effect has been attributed to the different resolved shear stress on the leading and trailing partial dislocations and the reduction of surface energy by twinning [13,14]. DT is conventionally not expected for bulk Au and other fcc metals at room temperature and experimental strain rates [2,28]. However, in the absence of easy sources of dislocations, the initial process for both ODP and DT is the nucleation of a leading partial dislocation from the surface. The self-stimulated emission of twinning partial dislocations at the intersection of the partial dislocation with the surface edges

Fig. 5. View along the $[-1\,0\,1]$ direction on the whiskers. Atoms are colored according to their coordination number (magenta: 9; grey: 8). Left: after $\varepsilon_p = 4\%$ plastic strain; right: after fracture. The pristine whisker accommodates strain by many small twins and fails before a long twin forms. The predeformed whisker accommodates strain by fewer twins. A long twin can form, which tilts away from the untwinned part of the whisker after fracture. The whisker with rough surfaces accommodates the same plastic strain by few, long twins, and the whisker fails after nearly its entire length has undergone twinning. (For interpretation of the references to colour in this figure legend, the reader is referred to the web version of this article.)
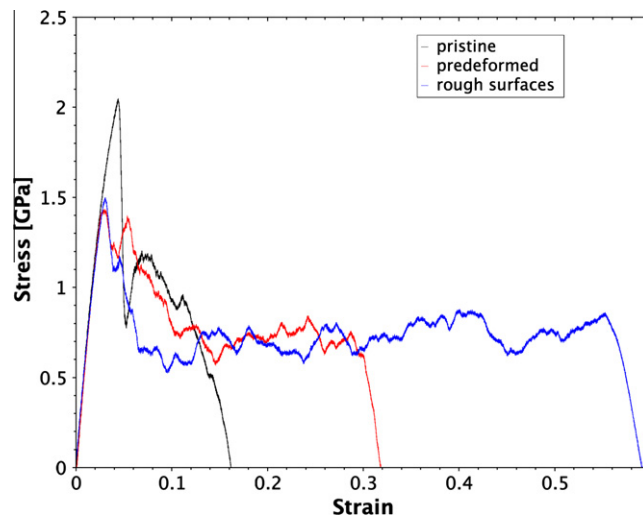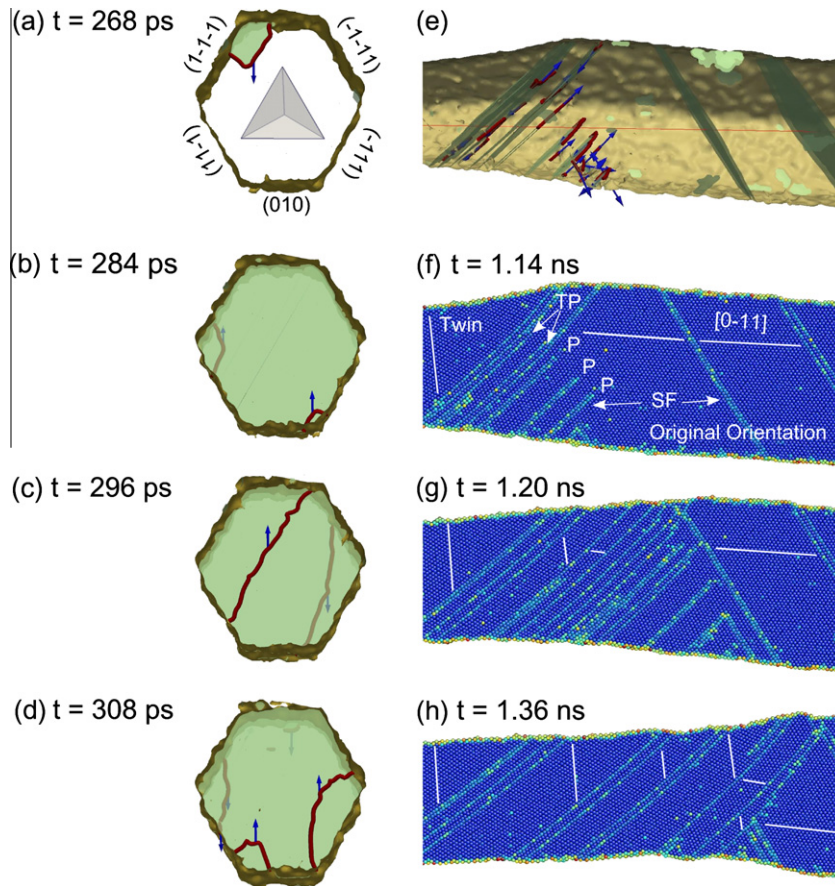
Fig. 7. Details of the twinning mechanisms in the wire with rough surfaces. (a–e) Show the result of the DXA analysis; the partial dislocation lines are red, the stacking and twin faults green and the Burgers vectors are denoted by blue arrows. (a–d) Show a view on the (1 1 1) plane, visualized by the Thompson tetrahedron, during the layer-by-layer twinning mechanism. Partial dislocations are nucleated at the edges between {1 1 1} and {1 0 0} surfaces. At the intersections of the stacking fault with surface edges, partial dislocations with the same Burgers vector are nucleated on atomically adjacent planes above and below the stacking fault. This process is self-sustaining and redundant, as twinning dislocations on the same plane can nucleate at different sites (d) and subsequently merge. (e–g) Show a view along the [−1 0 1] direction on twin deformation by leapfrogging partial dislocation (P) emission and formation of embryonic twins ahead of the main twin by emission of twinning partial (TP) dislocations. These subsequently merge together and with the main twin. Coloring in (f–h) according to the centrosymmetry parameter. (For interpretation of the references to colour in this figure legend, the reader is referred to the web version of this article.)

acts as a plane-to-plane promoter for the slip, as required by the "stimulated slip concept" for twinning [8]. The dominance of DT over ODP, however, furthermore requires that the stacking faults on which embryonic twins can form are not destroyed by subsequent nucleation of trailing partial dislocations. The size-dependence of partial vs. full dislocation activity has been previously modeled in terms of the ratio of the stable stacking fault energy γ_{sf} to unstable stacking fault energy γ_{usf} in the context of nc plasticity [29]. Similarly, the twinning tendency of various fcc metals is argued to depend on the stable and unstable twin fault energy γ_{tf} and γ_{utf} [28,30,31]. However, these approaches neglect possible differences in the work done by the resolved shear stress acting on the leading and trailing partial dislocations [13]. Moreover, many studies examine only specific loading conditions such as those at a crack tip [28,31–33]. The different resolved shear stresses on the leading partial and corresponding full dislocations can easily be incorporated in the expression of Chen et al. [3] for the

critical grain size D_c for DT in nc fcc metals. We accomplish this by including the Schmid factors for the full and the leading partial dislocation, m and m_{lp}, and the corresponding Burgers vectors b and b_p, giving the following expression:

$$D_c = \frac{2\alpha\mu\left(b\frac{m_{lp}}{m} - b_p\right)b_p}{\gamma_{SF}} \qquad (1)$$

where μ is the isotropic shear modulus and the factor α contains the character of the dislocation and a scaling factor between the length of the dislocation source and the crystal size. For the [1 0 1]-oriented whisker, the slip systems with the largest resolved shear stress has a Schmid factor of $m = 0.408$. The corresponding leading partial dislocation has a Schmid factor of $m_{lp} = 0.471$, whereas the trailing partial dislocation has a Schmid factor of $m_{tp} = 0.236$. With $\mu = 22.55$ GPa, $b = 2.885$ Å, $b_p = 1.666$ Å, $\gamma_{sf} = 31$ mJ m^{-2} as given in Ref. [24] and $\alpha = 1$, the critical grain size according to Eq. (1) would be of the order of $D_c = 40$ nm. As can

be seen in Fig. 5a, the dislocation source size is usually only a fraction of the crystallite size. The true critical size at which full dislocation activity is expected to take over partial dislocation activity is therefore many times larger than D_c.

For the reoriented [1 0 0] whisker, the slip system with the largest resolved shear stress has a Schmid factor of $m = 0.408$, but here the leading partial dislocation has a Schmid factor of $m_{lp} = 0.236$, which leads to $D_c \approx 0$, i.e. twinning is not expected in this geometry. This is in agreement with the simulations and experiments where the reoriented twinned regions did not show any twinning, but full dislocation activity as shown in Fig. 8. Overall, the predictions of D_c support the occurrence of twinning in [1 0 1], where $m_{lp}/m = 1.15$, as well as the absence of twinning in the re-oriented whisker in which $m_{lp}/m = 0.58$. This emphasizes the importance of the orientation of the loading axis with respect to the slip systems in addition to the material properties (stacking and twin fault energies) in determining whether ODP or DT will be the dominant deformation mechanism.

A key finding of our work is the observation of distinct manifestations of deformation twinning-mediated plasticity in these Au nanowhiskers. That twinning mediates plastic flow in nanoscale metals, not empirically known to undergo deformation twinning during laboratory testing conditions, underlies the importance of initial defect and flaw density and character. Our experiments and simulations indicate two different characteristic classes of plastic response that both operate near the ideal strength of Au, yet range from jerky and intermittent to smooth and quasi-continuous behavior. In most cases, fracture occurs only after substantial plastic strain (>5%), which, coupled with high strength, is suggestive of materials with very high tensile ductility.

In class I, partial dislocations readily nucleate and grow to $\Sigma 3$ (1 1 1)[1 0 −1] nanotwins (3–4 atomic planes thick) that are spatially distributed along the length of the nanowhisker, but do not generally continue to grow. Instead, nucleation and creation of new nanotwins on multiple slip systems are preferred. This mechanistic regime is supported
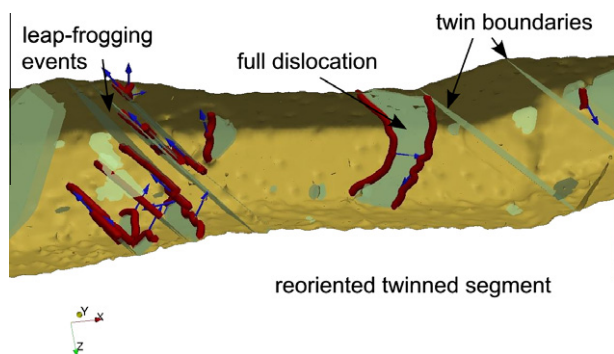

Fig. 8. DXA analysis of a snapshot from the pre-deformed whisker, showing the leapfrog propagation of a long twinned segment and a full dislocation in this reoriented twin.

by experimental observation of copious slip traces on multiple {1 1 1} planes and the absence of long continuous twinned regions that generally tilt away from the tensile axis following fracture. This class of plastic deformation morphology correlates with a stress–strain response that exhibits smooth yielding and continuous plastic flow, in contrast to the jerky and intermittent flow reported in Au micro- and nanopillar compression [34–37]. The requirement for this mode of twinning-mediated deformation is the suppression of the formation of long twinned regions of the whisker. MD simulations of pristine whiskers indeed show this qualitative behavior; an example of such a suppression mechanism includes interactions between growing twins that originate on conjugate slip planes. While the underlying reasons responsible for the experimentally observed behavior could be different from those present in MD simulations, the two modes of resulting deformation and concomitant twinning behavior are clearly delineated in both experiments and MD.

Class II response, which has emerged from both experiments and simulations, is clearly characterized by the growth of deformation twins to sizes that are appreciable fractions of the nanowhisker specimen. Atomistically, the formation of such long $\Sigma 3$ twins is correlated with changes in mechanisms. Rather than continuing the propagation of the twin boundary by layer-by-layer growth, leapfrogged nanotwins, stimulated by the internal bending stress (which depends on the applied load, the length and width of the twinned section, the crystal orientation and the lateral compliance of the specimen/machine assembly) coalesce with the primary twin boundary front. The result is a self-sustained and accelerated growth of the primary twin upon coalescing with leapfrogged nanotwins, which we deem a supercritical process since the magnitude of the internal bending stress increases with increasing twin length. We propose that a critical twin size exists, presumably larger than a nanotwin only a few atomic planes wide, for the internal bending stress to grow to a sufficient magnitude such as to initiate the leapfrogged nucleation events and accelerate the growth of the primary twin via this coalescence mechanism. Once this critical point is reached, then the twin growth proceeds at a constant stress level until it encounters some obstacle that inhibits further growth (e.g. a stacking fault or nanotwin on a conjugate slip plane), which can ultimately lead to nanowhisker rupture. In the special case where no obstacles are found, the entire specimen can reorient into a twinned configuration. A key morphological signature of such a twinned region is the rotation of the segments of the nanowhisker away from the tensile axis following fracture. This rotation is easily detected in nanowhisker tensile testing experiments (Figs. 2d and 3b), and the correlation with coordinated deformation twinning further corroborated by orientation mapping (Fig. 3). The concomitant stress–strain behavior in the case of facile twin growth contrasts with the continuous flow seen when dislocation slip, planar faults, and static nanotwins appear to be randomly distributed along the specimen.

The observation that two distinct manifestations of twinning-mediated plasticity produce such different mechanical response in nominally similar specimens is notable. Our experiments show no clear correlation between the mode of deformation and specimen cross-sectional area or aspect ratio. However, comparison of the atomistic simulations of pristine, rough and pre-defected nanowhiskers point to the importance of the spatial distribution of initial dislocation nucleation sites in controlling the ensuing mode of plastic deformation. The steps created by leading partial dislocations at the surfaces and in particular at surface edges provide nucleation sites for further (twinning) dislocations, which can be activated at significantly lower stresses. In the absence of sources with lower activation stresses, partial dislocations that nucleate first lead to the formation of the first twins, which in the simulations are also the dominating twins. The nucleation of partial dislocations at surfaces is expected to be thermally activated [38–40]. At the high strain rates of MD simulations, thermal activation plays only a marginal role, and therefore nucleation of partial dislocations in the pristine whisker takes place in a narrow strain window when the stress has reached the critical stress for dislocation nucleation at surface edges. Together with the elastic driving force, this leads to a relatively homogeneous spatial distribution of partial dislocations throughout the whisker. Many twins can form on top of their stacking faults (see Fig. 5), which subsequently interact with each other and form obstacles to further propagation of the twins. The formation of extended twins is therefore less probable, and the boundary between intersecting twins leads to early failure.

In contrast, when the distribution of nucleation sites includes a few sites with low critical stresses (e.g. in the simulation with surface roughness), the dominant twins will form on the stacking faults created by the first partial dislocations and accommodate most of the strain without encountering many obstacles produced during the deformation, like conjugated twins. This specimen can therefore almost entirely twin by the leapfrogging and coalescence mechanism. The behavior of the pre-deformed specimen lies between the pristine specimen and that with the random surfaces. The two pre-existing stacking faults act as preferred nucleation sites for partial dislocations, which in turn stimulate other dislocations, including twinning dislocations on the initial stacking faults. As a result, the plastic strain is accommodated by fewer, but thicker, twins as compared to the pristine whisker (see Fig. 5). Two of the larger twins trigger the accelerated mode of twin propagation. However, the longer twin intersects with a small twin on the conjugated plane, where the whisker fails. At this point, about two-thirds of the whisker have undergone twinning. After fracture the bending stress, superimposed by the tensile setup, is relieved and the twinned region tilts away from the matrix to meet the original shape relationship between twinned and untwinned region.

In experiments, the appearance of finite and positive strain hardening rates can be related to the consecutive nucleation of partial dislocations at seemingly random sites along the whisker. In long whiskers, the glide of individual partial dislocations and the formation of $\Sigma 3$ nanotwins contribute only by a small fraction to the overall plastic strain of the specimen and consequently do not release a large amount of strain energy. Provided that the nucleation strengths of all sites are statistically distributed or that nucleation is thermally assisted [38–40], then the measured plastic flow can commence in a markedly smooth fashion as the density of individual planar faults and nanotwins increases with increasing plastic strain. The statistical sampling of nucleation strengths may lead to the observed apparent strain hardening.

5. Conclusion

We present in situ tensile tests and MD simulations of nominally defect-free $\langle 110 \rangle$ oriented Au nanowhiskers. At room temperature and quasi-constant strain rates of 10^{-4} s^{-1} these specimens show yield stresses near the ideal strength and significant amounts of plastic strain between 5% and 12%. TEM and EBSD investigations identify deformation twinning as the dominant deformation process, which leads either to the formation of a large number of small twins distributed along the length of the whisker or the formation of one long twin. These two deformation modes correspond to two classes of stress–strain curves, with the former demonstrating continuous flow, and the latter showing pronounced stress drops. MD simulations suggest that the two deformation modes correspond to two distinct mechanisms of twin propagation, namely self-stimulated layer-by-layer growth or growth and coalescence of leapfrogging nanotwins formed on the stacking faults of stimulated partial dislocations leading the main twin. We hypothesize that the accelerated propagation mode is induced by the bending moment due to a sufficiently long twin in combination with the boundary conditions. The existence of sufficiently long twins is favored by the heterogeneous spatial distribution of the nucleated twins and the lack of obstacles to twinning. Deformation twinning itself depends strongly on the differences of resolved shear stresses on leading and trailing partial dislocations and on the absence of pre-existing dislocations and easy dislocation sources. Taken as a whole, the ability of single crystalline Au nanowhiskers characterized by high crystalline quality to both withstand stresses near the ideal limit and accommodate large amounts of plastic strain as a result of deformation twinning, represents a shift from the dichotomy between high strength and toughness that governs bulk engineering materials.

Appendix A. Supplementary material

Supplementary data associated with this article can be found, in the online version, at http://dx.doi.org/10.1016/j.actamat.2012.03.018.

References

[1] Hirth JP, Lothe J. Theory of dislocations. New York: Wiley; 1982.
[2] Meyers MA, Vohringer O, Lubarda VA. Acta Mater 2001;49:4025.
[3] Chen MW, Ma E, Hemker KJ, Sheng HW, Wang YM, Cheng XM. Science 2003;300:1275.
[4] Oh SH, Legros M, Kiener D, Gruber P, Dehm G. Acta Mater 2007;55:5558.
[5] Seo JH, Yoo Y, Park NY, Yoon SW, Lee H, Han S, et al. Nano Lett 2011;11:3499.
[6] Zheng H, Cao AJ, Weinberger CR, Huang JY, Du K, Wang JB, et al. Nat Commun 2010;1:144.
[7] Lu Y, Song J, Huang JY, Lou J. Adv Funct Mater 2011;21:3982.
[8] Yu Q, Shan ZW, Li J, Huang XX, Xiao L, Sun J, et al. Nature 2010;463:335.
[9] Ogata S, Li J, Yip S. Phys Rev B 2005;71:224102.
[10] Zhang JY, Liu G, Wang RH, Li J, Sun J, Ma E. Phys Rev B 2010;81:172104.
[11] Asaro RJ, Suresh S. Acta Mater 2005;53:3369.
[12] Sansoz F, Huang HC, Warner DH. JOM 2008;60:79.
[13] Park HS, Gall K, Zimmerman JA. J Mech Phys Solids 2006;54:1862.
[14] Ji CJ, Park HS. Nanotechnology 2007;18:305704.
[15] Yamakov V, Wolf D, Phillpot SR, Gleiter H. Acta Mater 2002;50:61.
[16] Bachurin DV, Gumbsch P. Acta Mater 2010;58:5491.
[17] Deng C, Sansoz F. ACS Nano 2009;3:3001.
[18] Leach AM, McDowell M, Gall K. Adv Funct Mater 2007;17:43.
[19] Richter G, Hillerich K, Gianola DS, Mönig R, Kraft O, Volkert CA. Nano Lett 2009;9:3048.
[20] Gianola DS, Sedlmayr A, Mönig R, Volkert CA, Major RC, Cyrankowski E, et al. Rev Sci Instrum 2011;82:063901.
[21] Gianola DS, Eberl C. JOM 2009;61:24.
[22] Bitzek E, Koskinen P, Gahler F, Moseler M, Gumbsch P. Phys Rev Lett 2006;97:170201.
[23] Hoover WG. Phys Rev A 1985;31:1695.
[24] Park HS, Zimmerman JA. Phys Rev B 2005;72:054106.
[25] Stukowski A, Albe K. Model Simul Mater Sci 2010;18:085001.
[26] Kelchner CL, Plimpton SJ, Hamilton JC. Phys Rev B 1998;58:11085.
[27] Bitzek E. J Solid Mech Mater Eng 2012;6:99.
[28] Warner DH, Curtin WA, Qu S. Nat Mater 2007;6:876.
[29] Van Swygenhoven H, Derlet PM, Froseth AG. Nat Mater 2004;3:399.
[30] Jin ZH, Dunham ST, Gleiter H, Hahn H, Gumbsch P. Scripta Mater 2011;64:605.
[31] Tadmor EB, Hai S. J Mech Phys Solids 2003;51:765.
[32] Hai S, Tadmor EB. Acta Mater 2003;51:117.
[33] Rice JR. J Mech Phys Solids 1992;40:239.
[34] Greer JR, De Hosson JTM. Prog Mater Sci 2011;56:654.
[35] Volkert CA, Lilleodden ET. Philos Mag 2006;86:5567.
[36] Greer JR, Oliver WC, Nix WD. Acta Mater 2005;53:1821.
[37] Kraft O, Gruber PA, Monig R, Weygand D. Annu Rev Mater Res 2010;40:293.
[38] Nguyen LD, Baker KL, Warner DH. Phys Rev B 2011;84:024118.
[39] Ryu S, Kang K, Cai W. Proc Natl Acad Sci USA 2011;108:5174.
[40] Zhu T, Li J. Prog Mater Sci 2010;55:710.